Journal of
Materials Chemistry C

PAPER

View Article Online
View Journal | View Issue

Cite this: J. Mater. Chem. C, 2015, 3, 6745

Fabrication of highly efficient resonant structure assisted ultrathin artificially stacked Ag/ZnS/Ag multilayer films for color filter applications†

Garima Kedawat,*[ab] Pawan Kumar,[cd] Y. K. Vijay[a] and Bipin Kumar Gupta*[c]

Received 10th March 2015,
Accepted 1st June 2015

DOI: 10.1039/c5tc00678c

www.rsc.org/MaterialsC

We introduce a novel strategy for the fabrication of mechanically and thermally stable highly efficient resonant structure assisted ultrathin artificially stacked Ag/ZnS/Ag multilayer films on cleaned glass substrates using the thermal evaporation technique. The application of fabricated color filters has been studied in the visible range. These multilayers have good adhesion to each other and to the glass substrate, resulting in mechanical and thermal stability. The stability has been examined by the "Scotch-tape" test and the ultrasonication process at 37 kHz frequency and at 40 °C temperature as well as by thermogravimetric analysis (TGA). The results of the structural analysis, surface morphology and atomic force microscopy of these filters confirm the good crystallinity with a low value of surface roughness. The effect of thickness of artificially stacked metal (Ag) and dielectric (ZnS) layers has been examined in terms of optical properties by several spectroscopic techniques. These ingenious filters exhibit a large and deep stop band in the visible wavelength region. Thus blue, green and red color filters, centered at 460, 540 and 620 nm having bandwidths of about 25, 44 and 35 nm, respectively, were achieved. Moreover, the statistical outcomes of all the three filters (blue, green and red) show that the peak transmission efficiencies are consistently 73%, 70% and 63%, respectively. Additionally, the effect of different angles of incidence on the transmittance spectra has also been presented. Hence, the obtained results strongly suggest that these filters can be potentially used for tuning the color of optical filters according to the desired applications.

1. Introduction

Color filter devices possessing the characteristic of selective transmittance are capable of passing a certain portion of the visible wavelength spectrum while suppressing the other part of the spectrum. These filters have been regarded as an indispensable component in a variety of applications, such as fluorescence imaging, multi-spectral sensors, display devices and light emitting diodes.[1–4] The current research on the color filters is mainly focused on developing a smaller, faster and lower power design as compared to the commonly accessible designs. There are various important factors that played a key role in color filters in which, the most important aspect of color filters is the efficient use of light and enhancement of color saturation. Mainly, this research is based on the fundamental concept of the Fabry–Perot principle[5–7] to design artificially stacked ultrathin color filters of high transmissivity so as to promote their competitiveness in terms of their portable size, cost-effective fabrication and high packing density with lower gravimetric mass. Additionally, the ultrathin multilayers having strong in plane bonding forces offer harder coating resistance to extract individual layers as compared to bulk materials.[8] These layers consist of both periodic and symmetric geometries of metal (M)/dielectric (D)/metal (M) multilayer resonant structures. These are also known for the transparent metallic structure due to their highly transmissive window within a visible range of electromagnetic wavelength spectra.[9,10]

Additionally, highly transparent metallic structures have attractive potential applications as optical filters with high out-of-band rejection,[5,6,11,12] thin film metal electrodes in organic light emitting diodes,[13] nonlinear photonics,[14] electromagnetic shielding,[15] plasmonic nanoresonators mediated spectral imaging,[16–18] waveguides[19] and cavity induced optical filters.[20] These films are of great interest because (i) metal is very efficient to reflect light at infrared wavelengths and beyond

[a] Department of Physics, University of Rajasthan, Jaipur, 302055, India. E-mail: kedawat08@gmail.com; Fax: +91-11-45609310; Tel: +91-11-45609385
[b] Department of Physics, Kalindi College, University of Delhi, New Delhi, 110008, India
[c] CSIR – National Physical Laboratory, Dr K S Krishnan Road, New Delhi, 110012, India. E-mail: bipinbhu@yahoo.com
[d] Academy of Scientific and Innovative Research (AcSIR), CSIR – National Physical Laboratory campus, New Delhi – 110012, India

† Electronic supplementary information (ESI) available. See DOI: 10.1039/c5tc00678c

and (ii) at the same time, it is possible to make fairly efficient band pass filters with a minimum band width, despite the high imaginary part of refractive index of metals[9,10] and provide a large index contrast to low-absorptive dielectrics. Thus, an appropriate thickness of dielectric layers into two high reflective metal layer structures exhibits the resonant tunneling mechanism to open up the transmission windows for allowing the extraordinary transmission within a controllable spectral range, even though the total thickness of the metal layers significantly exceeds the skin depth.[10,11] These devices take advantage of the fact that the resonator structures filter out the colors on the basis of multiple reflections, interference and resonances between the optical modes of the cavity layer. The dielectric layer (that shows high transmittance in the visible region) sandwiched between the two highly reflective metal layers (that would otherwise be opaque to the visible region) improves the high optical transmittance in the visible wavelength region because of the refractive index discrepancy between the dielectric and thin metal layers.[21] This enhancement of optical transmittance characteristics is a function of the collective properties of individual components of layered coatings (*e.g.* density, refractive index and homogeneity) and their physical configuration (*e.g.* layer thickness and microstructure). The thickness also plays a direct impact on the filter's band-width and maximum peak transmittance. The choice of materials also plays an important role in the fabrication of color filters using ultrathin multilayer films. It depends on the adhesion between the thin layers and to the substrate, environmental stability, reproducibility, required spectral ranges and widths.

Zinc sulfide (ZnS) has a high refractive index (n = 2.35 at a wavelength of 560 nm), high transmittance (>90% in the visible wavelength range) and high electrical conductivity.[22] Furthermore, ZnS films can be deposited directly through vacuum heat evaporation with economic production costs and the facile synthesis process which can be used for a mass-scale. It can be potentially used as a dielectric material for M/D/M multilayer structures. In this series, silver (Ag) can be better alternative and suitable metal material due to its lower absorption in the visible part, frequency dependent refractive index and small thin-film resistivity for multilayer films.[23,24] Selectively, Ag is interesting to use because its interband absorption peaks lie above the visible spectrum which opens the possibility of broadband applications in the visible part of the spectrum.[9,10] The optical properties are also strongly influenced by the thickness, deposition conditions and dispersion of Ag film.[25,26] The Ag film should be thin, uniform and continuous for high transmittance in multilayer structures. In addition to this, the material and deposition procedure of Ag and ZnS thin films can be compatible with the state-of-the-art thin film color filter design process. The Ag/ZnS/Ag multilayer film composition has been investigated and reported by previous researchers.[27–29] The optical properties of Ag/ZnS/Ag multilayer structure usually depend on the positions of the metal layers and on the thicknesses of metal and dielectric layers. The photoluminescence (PL) emission of the surface plasmon metals (Ag, Al, *etc.*) is also another subject of interest in the current scenario.[30–33] More recently, plasmonic color filters were demonstrated by few research groups, where they exhibited filtering functionality in the visible range.[5,34–37] However, to the best of our knowledge, the dependencies of the optical properties of Ag/ZnS/Ag with varying thickness of metal and dielectric layers have not been studied to date, even when such artificially stacked layers can play a key role in the design of color filters with high optical transmissivity. The configuration of proposed color filters is illustrated in Fig. S1 (see ESI†). When light passes through this color filter, it reflects light of other wavelengths which is further recycled; however, when the light reaches a specific wavelength, then it is transmitted through the medium. In the designed color filter, an ultrathin ZnS dielectric film is formed between the two Ag films. The top and bottom Ag film is in contact with air and a glass substrate, having nearly constant refractive indices of 1 and 1.5 with a negligible loss, respectively. The notations of structural parameters are denoted as t and d, where t represents the thickness of Ag and d corresponds to the thickness of the ZnS layer. The refractive indices for the dielectric and metal films are represented as n_d and n_m, respectively.

In this paper, we report on mechanically and thermally stable ultrathin visible wavelength color filters that take advantage of symmetric metal/dielectric/metal (Ag/ZnS/Ag) multilayer resonant structure films. Thermal and mechanical stability are highly desired for long term practical application of these filters in optoelectronic devices to avoid any kind of degradation in optical filters due to the thermal and mechanical damage being caused. We have addressed such issues in our present investigation, which have been merely reported so far. The transmittance of multilayer resonant structure is rigorously analyzed by taking into account the different thicknesses of metal and dielectric layers. Furthermore, we have also studied and discussed the angular dependency on the transmittance spectra. We have also focused on the design and fabrication of three different blue, green and red color filters relying on an ultrathin metal/dielectric/metal resonant structure (Ag/ZnS/Ag), exhibiting polarization dependence and high transmission efficiencies ranging from 73–63% for blue to red color filters. Additionally, we also explored the PL emission properties of ultrathin artificially stacked Ag/ZnS/Ag multilayer film.

2. Experimental

2.1 Fabrication of ultrathin Ag/ZnS/Ag multilayer films

The ultrathin Ag/ZnS/Ag multilayer films were prepared using the thermal evaporation technique under high vacuum on cleaned glass substrates. ZnS (99.99%, high purity) in the granular form and Ag (99%, high purity) in the wire form having 1 mm diameter were kept on tantalum boats separately. The deposition rates for ZnS and Ag were (2.00 ± 0.10) Å s^{-1} and (3.00 ± 0.15) Å s^{-1}, respectively. The thickness of dielectric layers in the center of structure was set higher than that of two outer metal layers. This design structure is based on the theory that when a light beam is incident on the structure, it induced

Table 1 The optimized design of Ag/ZnS/Ag multilayer thin film structures

	Optimized structure thickness (nm)		
Sample no.	Air/Ag	ZnS	Ag/substrate
1	25	85	25
2	30	85	30
3	35	85	35
4	40	85	40
5	32	55	32
6	32	65	32
7	32	75	32
8	32	85	32
9	32	95	32

transmittance at certain wavelengths and rejected other wavelengths, by metal layers. The film thickness was controlled during the deposition by a quartz crystal thickness monitor. In order to gain a better understanding of the M/D/M multilayer resonant structures and the effect of individual design parameters on the resulting transmittance and reflectance spectra, the systematic studies were first performed by varying the individual thickness of each layer. This was followed by an optimization process that improved the transmittance spectrum by independently adjusting the thickness of each layer in the structures. Thus, the color filters were obtained at a particular thickness of dielectric and metal layers. The optimized design of ultrathin Ag/ZnS/Ag multilayer films on glass substrates is presented in Table 1. In this study, the monochromatic wavelength spectrum values for blue, green and red light are defined as 460, 540 and 620 nm, respectively, to design the color filters.

2.2 Characterization

The structure of thin films was studied in terms of X-ray diffraction (XRD) patterns, recorded using a PANalytical X'pert PRO X-ray diffractometer with Cu Kα_1 radiation (λ = 1.5406 Å). The surface morphology of thin films was investigated by atomic force microscopy (AFM) using a Vecco Instruments CP II. The surface topography was characterized from the field emission scanning electron microscopy (FESEM) image using a microscope of Carl ZEISS-SUPRA 40 at 5 kV operating voltage. The microstructural studies were carried out using high-resolution transmission electron microscopy (HRTEM, Model No. Technai G20-twin, 300 kV with super twin lenses having a point and line resolution of 0.144 nm and 0.232 nm, respectively) equipped with energy dispersive X-ray analysis (EDAX) facility. Raman scattering experiments were carried out at room temperature using a Renishaw 1000 with a Leica Microscope DM LM. The light was focused to a ~1 μm spot and the backscattered light was analyzed using laser excitation at 514.5 nm from an Ar^+ laser. The photoluminescence (PL) characterization of thin films was carried out using a luminescence spectrometer (Edinburgh, FLSP – 920) with an EPL 375 nm picosecond pulsed diode laser as a source of excitation. The PL mapping of thin films was performed using a WITech alpha 300R + Confocal PL microscope system (WITech GnBH, Ulm, Germeny), where a 375 nm diode laser was used as a source of excitation. The UV-Vis spectra of multilayer thin films were recorded using a dual beam Hitachi U3300 spectrophotometer in the visible spectral range with different angles of incidence. The contact angle measurement was carried out using a drop shape analysis system, DSA 10 Mk2. TGA was performed using a Perkin-Elmer TGA-7 in an air atmosphere at a heating rate of 10 °C min^{-1} from 30–800 °C. The surface roughness was recorded using atomic force microscopy (AFM) (model: NT-MDT Solver Scanning probe Microscope). The ultrasonication bath treatment was performed using a S15 H Elmasonic instrument at 37 kHz frequency and at 40 °C temperature.

3. Results and discussion

The gross structural analysis and phase purity of ultrathin artificially stacked Ag/ZnS/Ag multilayer film were determined by XRD to exploit the presence of Ag and ZnS lattices. Prior to the XRD measurements, the calibration of the diffractometer was done with silicon powder (d_{111} = 3.1353 Å).[38] Fig. 1a shows the XRD pattern of Ag/ZnS/Ag multilayer thin film (sample 2; details are given in Table 1) and the inset shows the photograph image of Ag/ZnS/Ag multilayer thin film. The XRD pattern exhibits peaks at 2θ angles of 28.775°, 47.956°, and 56.765° corresponding to the (002), (110) and (112) planes of the hexagonal wurtzite phase of ZnS, respectively. It is in good agreement with the standard data (JCPCS card No. 36-1450, lattice parameters $a = b$ = 0.3820 nm, and c = 0.6257 nm). The diffraction peaks at 2θ angles of 38.440°, 44.547°, and 64.750° correspond to the (111), (200) and (220) plane orientations of the cubic phase of Ag, respectively, which is comparable to the standard value (JCPDS card No. 04-0783, lattice parameters $a = b = c$ = 0.4086 nm). The peaks represent the crystallographic nature of multilayer thin film. No additional peaks as well as secondary phases are found in the combined multilayer structure of Ag/ZnS/Ag film, except pristine ZnS and Ag peaks, which show the purity of multilayer thin film. Lattice diffusion does not occur during the fabrication of multilayers, which is further

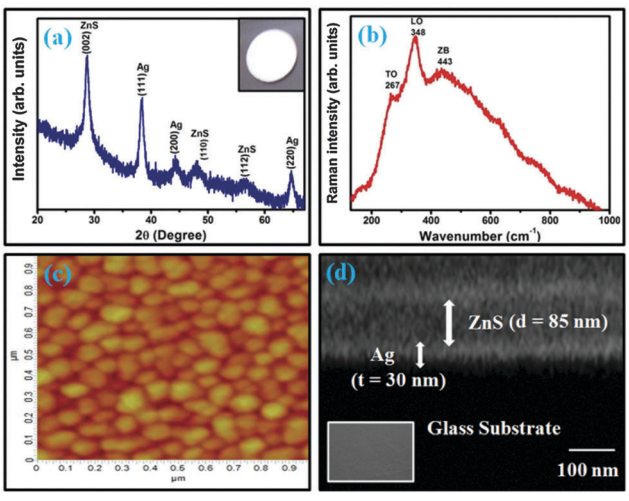

Fig. 1 (a) XRD pattern; the inset shows the deposited film, (b) Raman spectrum, (c) 2D AFM image (sample 2) and (d) cross-sectional SEM image; the inset shows the top surface image of Ag/ZnS/Ag multilayer thin film of sample 2 (details are given in Table 1).

evidenced by the SEM image. The particle size is estimated using Scherrer's formula and is found to be 10–15 nm with respect to the highest peak intensity observed for the multilayer film.

Raman spectroscopy was examined to confirm the crystalline structure of multilayer films. Fig. 1b shows the Raman spectrum of Ag/ZnS/Ag multilayer thin film (sample 2). The dominant peak at 348 cm^{-1} and the weaker peak at 267 cm^{-1} are associated with the longitudinal optical (LO) phonon and transverse optical (TO) phonon peak of the hexagonal phase of ZnS, respectively. In addition, a broader band peak near 443 cm^{-1} is also observed with the zone boundary (ZB) phonon, due to the plasma-enhanced resonant Raman effect. Only the peaks which correspond to the hexagonal wurtzite phase of ZnS have appeared. Metal Ag has a cubic structure that does not show any first order Raman spectrum which was expected. The appearance of these phonon features such as phonon softening and line broadening of the Raman peaks is due to the quantum confinement effects in nanocrystal thin films.[39] The 2D AFM surface topological image at a scale size of 1 × 1 μm of artificially stacked Ag/ZnS/Ag multilayer thin film (sample 2) is shown in Fig. 1c. The surface of thin film shows a uniform and smooth surface with a mixture of small and large grains. The average root mean square (RMS) roughness value is estimated to be around 4–6 nm. The roughness of the surface plays an important role in determining the optical properties of multilayer film. Because, the nature of the surface features provides valuable information about the interactions of light with the surface of the layer that how light will be absorbed and scattered or diffracted by such a surface.

The 2D AFM surface topological image of artificially stacked Ag/ZnS/Ag ultrathin multilayer film (sample 2) is also obtained after 24 hours and 3 months of deposition time, which is shown in Fig. S2a and b (see details in the ESI†). It reveals that the surface roughness is not affected after 3 months of deposition time. It means that the ultrathin films are stable after 3 months. The top-view SEM images of Ag/ZnS and Ag/ZnS/Ag are also depicted in Fig. S3a and b (see details in the ESI†). It is observed that both films confirm the uniform and homogeneous surface composed of closed packed nanometric grains or crystallites. Fig. 1d shows a cross-sectional backscatter scanning electron microscopy (BSD SEM) image of Ag/ZnS/Ag multilayer thin film (sample 2). This image confirms the three alternate artificially stacked layers of Ag and ZnS which are uniformly deposited on glass substrate. The light grey band represents the typical SEM image of the Ag layer and the dark grey band exhibits the ZnS layer, with a thickness of ~30 ± 2 nm and ~85 ± 2 nm for the Ag and ZnS layer, respectively. The inset of Fig. 1d shows the SEM image of the top surface of Ag/ZnS/Ag multilayer thin film which represents that the Ag particles are uniformly distributed on the ZnS thin layer. We have also investigated the cross-sectional morphology of another artificially stacked multilayer film through the SEM technique (Fig. S4; see details in the ESI†) in which this image confirms the uniform deposition of three layers Ag/ZnS/Ag on glass substrates. In Fig. S4 (ESI†), 1 and 3 represent the Ag layers and 2 indicates the ZnS layer. The light grey parts show the interface between the two deposited layers.

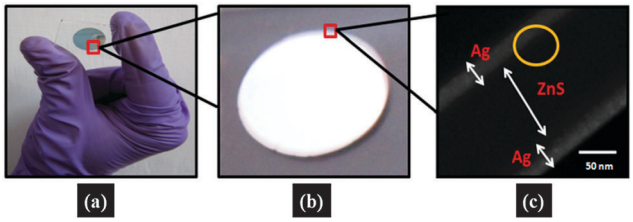

Fig. 2 (a) Optical picture of Ag/ZnS/Ag multilayer thin film and (b) close view of thin film of (a) and (c) cross-sectional TEM image of multilayer alternate films of Ag and ZnS of sample 2 (details are given in Table 1). The yellow marked circle (in (c)) represents the interface between Ag and ZnS layers.

To examine the detailed microstructure information, we have performed high-resolution transmission electron microscopy on ultrathin multilayer films. Fig. 2a represents the optical picture of artificially stacked Ag/ZnS/Ag film and the close view of the optical filter is shown in Fig. 2b. Fig. 2c clearly shows the cross-sectional TEM image of artificially stacked multilayer alternate films of Ag and ZnS (sample 2). The bright and dark bands represent the Ag and ZnS layer, respectively. The estimated thicknesses of Ag and ZnS layers in the composite system are ~30 nm and ~90 nm, respectively. It clearly shows that the thicknesses of designed and deposited films are quite consistent. The interface between the two deposited layers is well-defined, which can be clearly seen in Fig. 2c, by the yellow marked circle.

Mechanical stability has been obtained by the "Scotch-tape" test. The "Scotch-tape" test was an effective tool for demonstrating the stark difference in adhesion between the layers. The "Scotch-tape" test was used to examine the adhesive strength of the artificially stacked Ag/ZnS/Ag multilayer film (sample 2) to the glass substrates (Fig. 3a and b). The "Scotch-tape" was applied to the surface of multilayer film (Fig. 3c) and coating film was pressed by forceps (Fig. 3d) and then, slowly pulled off the tape using forceps through the hand (Fig. 3e). After removing the tape, the coating layer is not affected (Fig. 3f). Any delaminating parts are not removed from the substrate, which is left on the adhesive tape if the coating layer

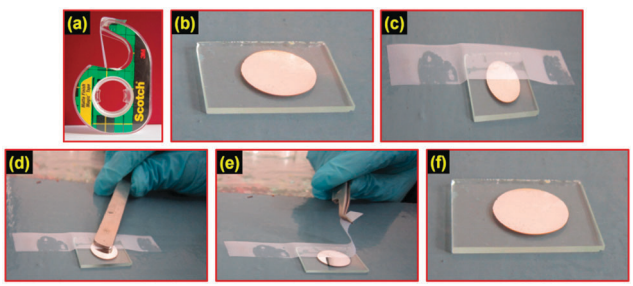

Fig. 3 Application of the "Scotch-tape" test to the artificially stacked Ag/ZnS/Ag multilayer film for measuring the mechanical stability; optical image of (a) Scotch-tape, (b) Ag/ZnS/Ag multilayer film, (c) applied a Scotch-tape to the Ag/ZnS/Ag multilayer film, (d) pressed the coating film by forceps, (e) pulled off the tape using forceps through the hand and (f) Ag/ZnS/Ag multilayer film after removing the tape, resulting in no delamination of film and mechanical stability was observed.

is not stable with the glass substrate. As a result, the adhesiveness of the coating thin film to the glass substrate is very strong. The stability adhesion of the ultrathin film with the glass substrate and between the Ag and ZnS layers is observed. Even after repeating the ''Scotch-tape'' test multiple times, the tape remained clean and no damage to the multilayer film coatings is noticeable. Thermal stability of ultrathin multilayer films has been analyzed by Thermo-Gravimetric Analysis (TGA), as shown in Fig. S5 (see ESI†). The hydrophobic nature of artificially stacked Ag/ZnS/Ag multilayer film and the ultrasonication bath treatment to the artificially stacked Ag/ZnS/Ag multilayer film for measuring the mechanical stability are given in Fig. S6 and S7 (see ESI†). The increment in interfacial adhesion strength between the glass and metal film (silver) is due to the inherent high surface energy of silver as compared to ZnS. This is the main cause to choose ZnS as an intermediate layer between the two silver layers to enhance the strength of the Ag/ZnS/Ag multilayer films. Although, Ag has good adhesion with the ZnS layer, which can be clearly seen from Fig. 3e. As a result, the overall thermal stability and mechanical strength of color filters enhanced greatly as compared to individual layers of Ag and ZnS with glass.

After examining the stability, it is also interesting to explore the plasmonic PL emission of Ag in Ag/ZnS/Ag multilayer thin film (sample 2) as well as defect induced PL emission emerging from the interface of Ag and ZnS thin films by PL spectroscopy. Fig. 4a shows the PL emission spectra of multilayer thin film with the xenon lamp as a source of excitation at 375 nm wavelength. The PL spectrum consisted of three peaks which are centered at 504, 613 and 645 nm. The peak at 504 nm corresponds to the band to band transition of Ag ultrathin film which is consistent with our earlier reported results[30] and another two peaks (613 and 645 nm) are related to Ag induced defects on the ZnS film surface. The visible green plasmonic emission at 504 nm originates due to the recombination of excited electrons present in the d orbital of Ag ($5s^14d^{10}$) with holes existing on the surface of ultrathin Ag film. The other two defect related PL peaks (613 and 645 nm) emerge due to interface formation between Ag and ZnS alternate layers. The observation of red emission from Ag/ZnS/Ag multilayer thin film is a very interesting result and it has been merely reported to date.[40] A red shift has been observed in signature peaks of ZnS (613 and 645 nm) due to interface formation between ZnS and Ag film.

Furthermore, we also examined the combined PL properties of plasmonic emission from Ag thin film as well as defect induced emission of Ag/ZnS/Ag multilayer thin film by PL mapping, which is recorded using a confocal PL mapping instrument with a 375 nm diode laser as a source of excitation. The sample was placed horizontally on the stub of the sample holder. We explored the top surface of Ag/ZnS/Ag multilayer thin film due to limitations of equipment. The optical micrograph image of Ag/ZnS/Ag multilayer thin film is shown in Fig. 4b. The two dimensional (2D), top view and three-dimensional (3D), lateral view of fluorescence mapping of

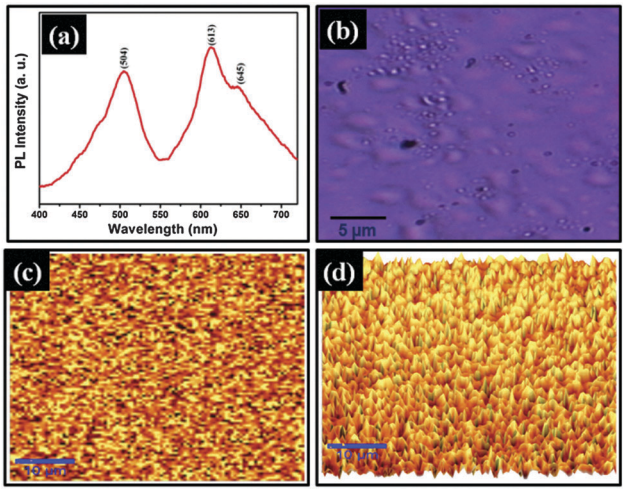

Fig. 4 (a) PL spectrum, (b) optical micrograph image, (c) 2D top view and (d) 3D lateral view of combined PL mapping of plasmonic emission from Ag thin film as well as defect induced emission of Ag/ZnS/Ag multilayer thin film (sample 2; details are given in Table 1).

Ag/ZnS/Ag multilayer thin film are shown in Fig. 4c and d, respectively. It arises due to plasmonic emission from Ag as well as defect induced emission of the Ag/ZnS/Ag multilayer. The obtained result reveals the uniform distribution of PL emission intensity in multilayer thin film. The optical micrograph image of another sample is shown in Fig. S8 (see ESI†). Furthermore, a systematic search is carried out in order to determine the effect of each layer on the optical properties of Ag/ZnS/Ag multilayer thin films. Thus, the transmissive properties of color filters are found out. The schematic representation of Ag/ZnS/Ag multilayer thin film structure for sample 2, each Ag and ZnS layer are found to be 30 and 85 nm thick, respectively, is shown in Fig. 5a. We have also compared the properties of this structure with those of single

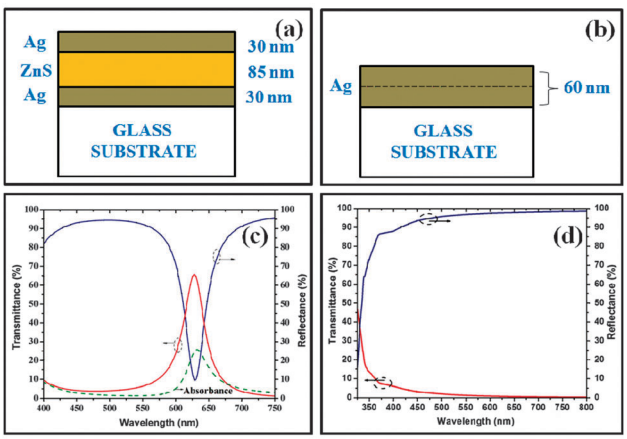

Fig. 5 (a) Schematic representation of Ag/ZnS/Ag multilayer thin film structure (sample 2, details are given in Table 1), (b) 60 nm thick Ag film on the glass substrate, (c) transmittance, absorbance and reflectance spectra of (a); and (d) transmittance and reflectance spectra of (b) at a normal angle of incidence.

thick Ag film that contains the same amount of Ag (60 nm thickness) as shown in Fig. 5b. The transmittance, reflectance and absorbance spectra of Ag/ZnS/Ag multilayer thin film (structure shown in Fig. 5a) and the transmittance and reflectance spectra of single layer Ag film (structure shown in Fig. 5b), as a function of incident wavelength for the normal angle of incidence, are shown in Fig. 5c and d, respectively. It has been found that the transmittance from the solid metallic Ag layer (structure and optical spectra are shown in Fig. 5b and d, respectively) is approximately in the order of $\sim 10^{-3}$ in the visible wavelength region. It exhibits low absorption and high reflectance in the visible part of the spectrum and fairly opaque to visible light and behaves like a mirror. On the other hand, embedding the dielectric layer (ZnS) between the two metal (Ag) layers (structure and optical spectra are shown in Fig. 5a and c, respectively), shows high transmittance in the visible region and blocks the ultraviolet and infrared wavelengths. The reflectance from the Ag layer is reduced to less than 5% and the absorbance dominated by the Ag layer is at a very low level. As a result, in spite of total thickness of Ag being much greater than its skin depth ($\sim$10–15 nm) in the visible region, the appropriate thickness of the ZnS layer between the Ag layers shows the interference and resonant tunneling effects, which open the high transmission windows in the visible regions. For example, 66% transmittance is obtained at 627 nm wavelength for sample 2, while the Ag metals are typically opaque for this wavelength. The other structures (as-mentioned in Table 1) also show the similar behavior.

The transmittance intensity of Ag/ZnS/Ag multilayer thin film structures also depends on the thickness of ZnS and Ag layers. Fig. 6a shows the transmittance spectral characteristics of designed Ag/ZnS/Ag multilayer structures for different thickness values of the Ag layer. Their optical performances are summarized in Table 2. It is clear from Table 2 that, for samples 1–4, the thickness of Ag layers increases from 25 to 40 nm in steps of 5 nm, under each ZnS layer thickness of 85 nm, new transmittance peaks appear one by one in the lower wavelength region of the spectrum with decreasing intensity from 72% to 48% and the fwhm (full width at half maximum) changes from 59 to 20 nm. The absorbance and reflectance spectra corresponding to these structures are also shown in Fig. S9 and S10 (see ESI†). For samples 5–9, the Ag layer thickness is fixed at about 32 nm and the effect of variation in ZnS layer thickness from 55 to 95 nm in steps of 10 nm on the transmittance of multilayer Ag/ZnS/Ag thin films is shown in Fig. 6b. The results are summarized in Table 2. It is clear from the table that the peaks shift towards the higher wavelength regions with decreasing intensity from 72% to 59% and the fwhm changes from 51 to 32 nm. The absorbance and reflectance spectra corresponding to these structures are also shown in Fig. S11 and S12 (see ESI†). The transmittance spectrum of Ag/ZnS/Ag multilayer thin film (sample 6) also depends on the oblique incidence of light, which is shown in Fig. 7. The spectral transmittance shifts toward shorter wavelengths when the angle of incidence (AOI) increases from normal incidence to higher angles (from 0° to 50°) and

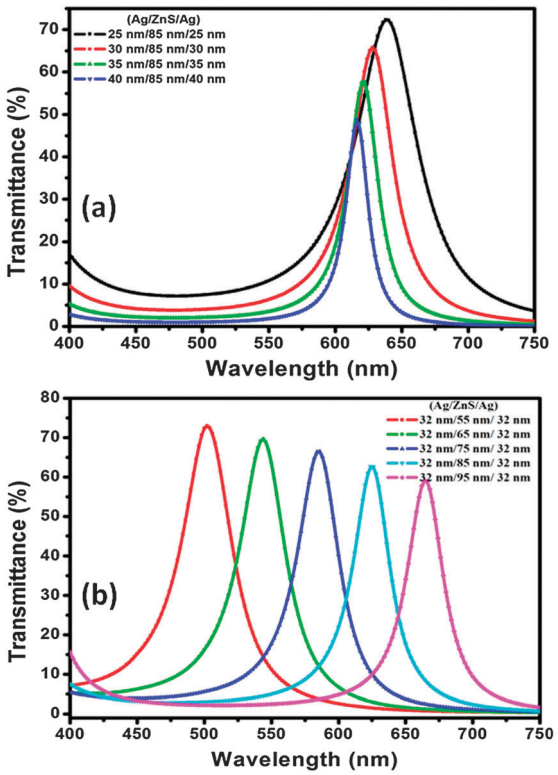

Fig. 6 Transmittance spectra of Ag/ZnS/Ag multilayer thin film structures (a) for varying the thickness of Ag (samples 1–4; details are given in Table 2) and (b) for different values of ZnS thickness (sample 5–9; details are given in Table 2) at a normal angle of incidence.

Table 2 The optical performance of Ag/ZnS/Ag multilayer thin film structures

Sample no.	Design structures Ag/ZnS/Ag (nm)	Peak wavelength (nm)	fwhm (nm)	Transmittance (%)
1	25/85/25	637	59	72
2	30/85/30	627	40	66
3	35/85/35	620	27	57
4	40/85/40	617	20	48
5	32/55/32	501	51	72
6	32/65/32	543	42	69
7	32/75/32	584	38	66
8	32/85/32	624	35	62
9	32/95/32	664	32	59

at the same time, the intensity of the peaks decreases from 69% to 58%. The fwhm also decreases from 42 to 35 nm, correspondingly. However, the filtered spectrum becomes highly distorted at higher angles, and also leads to a significant loss in performance and strong polarization dependence. When the AOI of light impinging on a filter is increased beyond normal incidence (0°), the resulting spectral shift can be described by eqn (1):

$$\lambda(\theta) = \lambda(0)\sqrt{1 - \sin^2(\theta)/n_{\text{eff}}^2} \quad (1)$$

where, θ is the angle of incidence and n_{eff} is called the effective index of refraction; this value is unique for each filter design and polarization state. This effect can be used to tune the filter

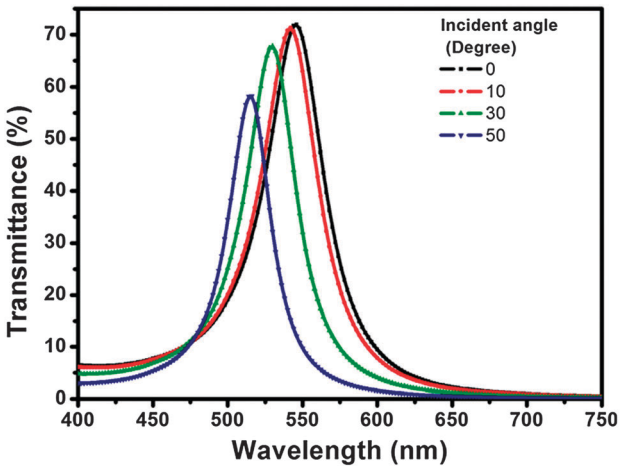

Fig. 7 Transmittance spectra of Ag/ZnS/Ag multilayer thin film (sample 6, details are given in Table 1) at different angles of incidence.

spectrum, albeit over a limited range. The blue shift is caused by the reduction of difference in the path length between the transmitted and reflected beams and the effective thickness of tilted thin film filters as compared to the horizontal films. Thus, the filter can always be adjusted to the desired spectral position by slight tilting.

Thus, from the above analysis, the ultrathin color filters can be designed using the fundamental concept of the Febry Perot principle. The three optimized designs of Ag/ZnS/Ag multilayer thin film structures for the primary colors, blue (B), green (G) and red (R), are listed in Table 3. The central wavelengths for B, G and R filters are at 460, 540 and 620 nm, respectively, to meet satisfactory color fidelity. From Fig. 8a, for the 460 nm wavelength, at 140 nm thickness of ZnS, 73% transmittance is observed. For the 540 nm wavelength (Fig. 8b), at 292 nm thickness of ZnS, there is optical transmittance at the 424 nm wavelength. It prevents the color from the pure green color. This may be due to the closing of the interference waveguide cycle. Therefore, the best thicknesses of ZnS thin films are 64 nm and 178 nm. For the 620 nm wavelength, in Fig. 8c, at 84 nm thickness of ZnS, the transmittance is 63% and for the 218 nm thickness of ZnS, an additional peak is obtained at 438 nm wavelength whose transmittance is 66%. This partial purple color side band approximately interferes with the transmittance of visible light; therefore, 84 nm thickness of ZnS is better for the design of red color filters. Thus, the above observations show that the best ultrathin film color filters, for the blue color filter, the film thicknesses are 32 nm/140 nm/32 nm and it has a maximum transmittance of 73% at 460 nm wavelength with a

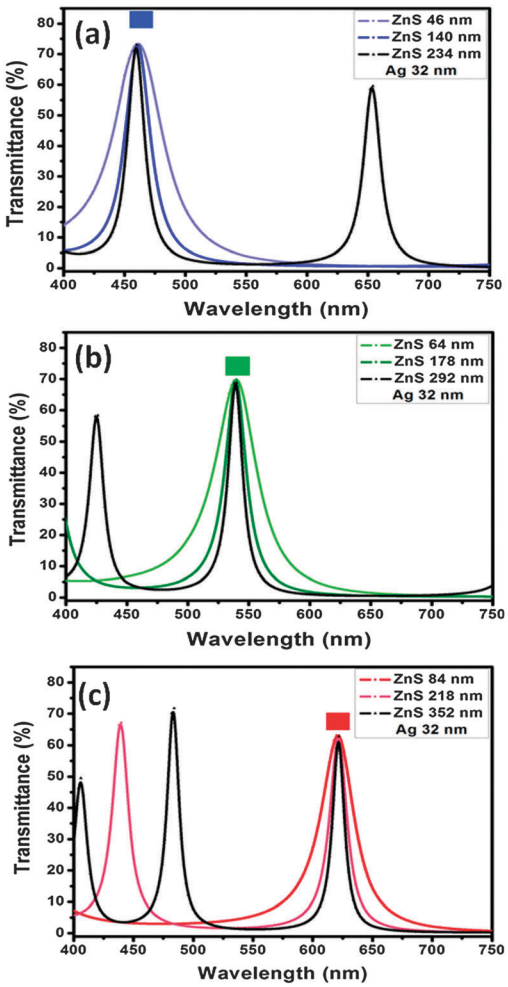

Fig. 8 Effect of the ZnS thickness on transmittance under a Ag thickness of 32 nm, (a) blue (460 nm wavelength) (b) green (540 nm wavelength) and (c) red (620 nm wavelength) color filters, and the inset shows color photographs of the structures viewed in transmission when illuminated with a diffuse white light source.

fwhm of 25 nm. For the green color filter, the film thicknesses are 32 nm/64 nm/32 nm and it has a maximum transmittance of 70% at 540 nm wavelength and a fwhm of 44 nm. For the red color filter, the film thicknesses are 32 nm/84 nm/32 nm and it has a maximum transmittance of 63% at 620 nm wavelength and a fwhm of 35 nm. Thus, this study infers that the enhancement of optical transmittance in a particular visible region depends on the refractive index and the thickness of metal and dielectric layers and it is helpful for the design of ultrathin film RGB color filters.

Fig. 9 shows the transmittance *vs.* wavelength characteristic curve for the green color filter at different angles of incidence.

Table 3 The optimized Ag/ZnS/Ag multilayer thin film structures for RGB color filters

Color filters	Design 1	Design 2	Design 3
Blue color filters (460 nm)	32 nm/46 nm/32 nm	32 nm/140 nm/32 nm	32 nm/234 nm/32 nm
Green color filters (540 nm)	32 nm/64 nm/32 nm	32 nm/178 nm/32 nm	32 nm/292 nm/32 nm
Red color filters (620 nm)	32 nm/84 nm/32 nm	32 nm/218 nm/32 nm	32 nm/352 nm/32 nm

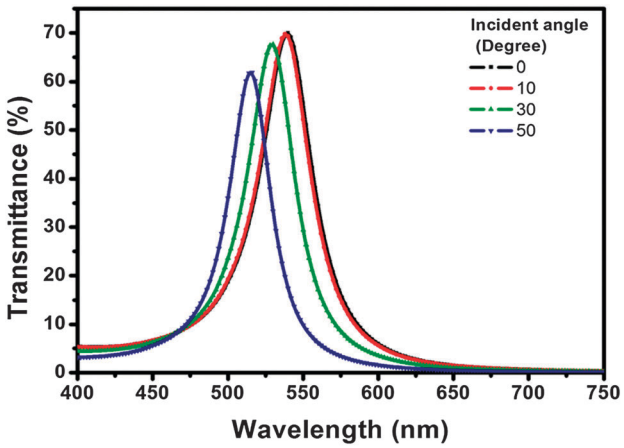

Fig. 9 Transmittance spectra of the green color filter at different angles of incidence.

This curve shows that as the angle between the sample and the beam changes by tilting the sample from 0° to 50°, the central wavelength exhibits a blue shift and at the same time, the intensity of the transmittance peaks decreases from 70% to 62%. These changes are also observed for blue and red color filters, as shown in Fig. S13 and S14 (see ESI†). Thus, these fabricated blue, green and red color filters could be an ultimate choice for the next generation tunable optical filters with portable size and advanced optical features. Moreover, the exceptional feature of these filters is that the attenuation of light can be achieved by changing the angle of incident beam on filters.

The cross-sectional scanning electron microscopy (SEM) images of Ag/ZnS/Ag multilayer thin films (blue color filters, green color filters, and red color filters) are shown in Fig. 10a–c. These images confirm that Ag and ZnS are uniformly deposited on glass substrates, alternatively. The light grey band represents the typical SEM image of the Ag layer having a thickness of ~30 ± 2 nm, 30 ± 2 nm, 30 ± 2 nm and the dark grey band exhibits the ZnS layer with a thickness of ~140 ± 2 nm, 65 ± 2 nm, 85 ± 2 nm, for blue color filters, green color filters, red color filters, respectively. These results also clearly indicate the thickness of each layer and interface between the Ag and ZnS layers. The qualitative analysis of artificially stacked ultrathin multilayer films of the red color filter was done using energy-dispersive X-ray analysis, as shown in Fig. 10d, which indicates the presence of the Ag, Zn and S elements in the multilayer structure, and Cu, C and O present due to the carbon-coated copper grid.

The cross-sectional SEM image of the red color filter was also used to study the quantitative analysis of the selectively spot area on individual layers, which has been examined on contrast individual bands of Ag and ZnS, as shown in Fig. S15 (see ESI†). Fig. S15a (ESI†) indicates the cross-sectional SEM image of red color filters, indicating the thickness of each layer and the interface between the Ag and ZnS layer. Fig. S15b and c (ESI†) show the weight % of each element present in individual layers of Ag (100%), Zn (50.8%), and S (49.2%) elements, respectively, which has been taken from Fig. S15a (ESI†), marked by the red cross-colored circle.

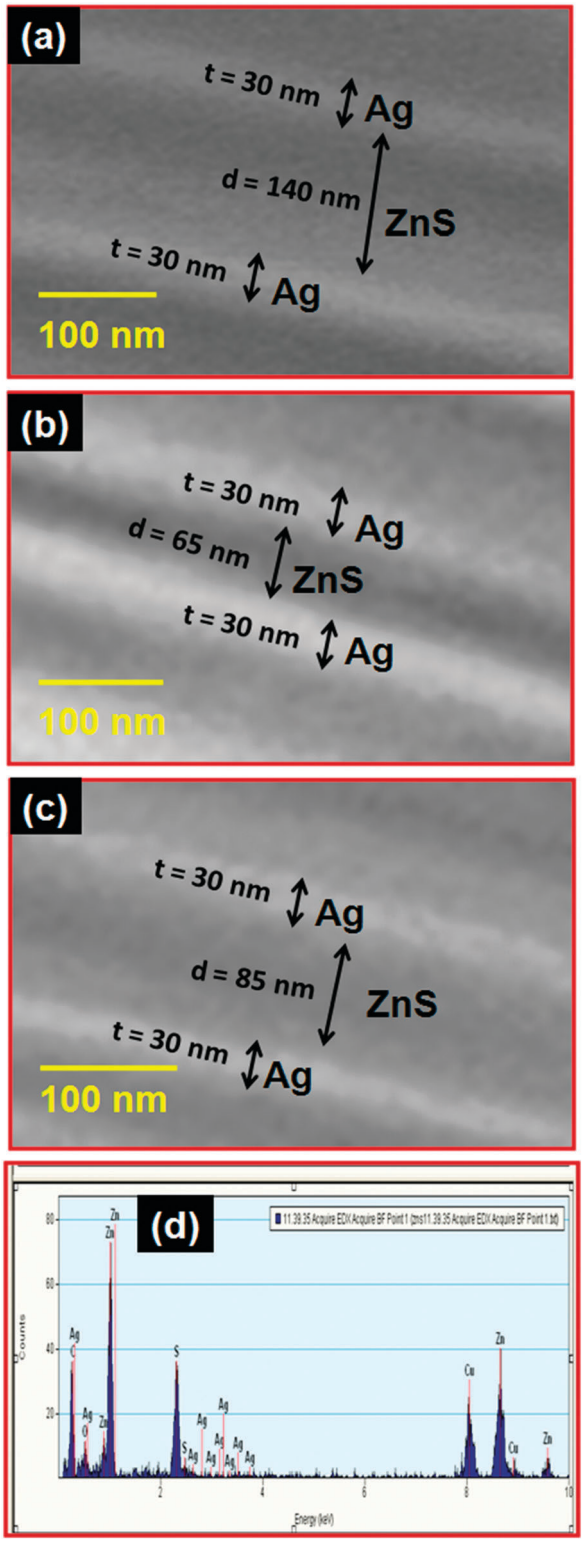

Fig. 10 Cross-sectional SEM images of Ag/ZnS/Ag multilayer thin films; (a) blue color filters (30 nm/140 nm/30 nm), (b) green color filters (30 nm/65 nm/30 nm), (c) red color filters (30 nm/85 nm/30 nm) and (d) EDX spectrum of red color filter multilayer thin film.

4. Conclusions

A novel strategy for the fabrication of mechanically and thermally stable and reproducible ultrathin RGB color filters with symmetric metal/dielectric/metal (Ag/ZnS/Ag) resonant structures is demonstrated using the thermal evaporation technique. These artificially stacked Ag/ZnS/Ag ultrathin multilayer structures have found to be strongly adhesive to the substrate and to each other, which is confirmed though the mechanical stability, thermal stability and contact angle measurements on Ag/ZnS/Ag ultrathin multilayer films. The artificially stacked Ag/ZnS/Ag ultrathin multilayer structures have shown transmission bands at visible wavelength that are highly tunable with respect to the thickness of the layers. The bandwidth and peaks of the transmission spectra are sought from the resonant characteristics of coupled metal-dielectric structure. The artificially stacked Ag/ZnS/Ag multilayer structures with their particular optical constants and thicknesses have shown good performance for color filter applications. The transmittances of 73%, 70% and 63% are observed for the blue, green, and red color filters at centered wavelengths of 460, 540 and 620 nm with corresponding bandwidths of 25, 44 and 35 nm, respectively. The transmittance spectra are also tunable with the change in the angle of incident beam on the sample. Thus, the proposed strategy for the fabrication of artificially stacked multilayers is highly suitable for its potential applications in advanced color tunable optical filters.

Acknowledgements

The authors wish to thank Director, N.P.L., New Delhi, for his keen interest in this work. The authors gratefully acknowledge University Grant Commission (UGC) Govt. of India for financial assistance and Department of Physics, University of Rajasthan, Jaipur (India) for experimental facilities to carry out this work. The authors are grateful to the CSIR-TAPSUN program for PL mapping facility.

References

1 F. J. Ko and H. P. D. Shieh, *Appl. Opt.*, 2000, **39**, 1159–1163.
2 Y. Cho, Y. K. Choi and S. H. Sohn, *Appl. Phys. Lett.*, 2006, **89**, 051102.
3 Q. Wang, D. Zhang, B. Xu, Y. Huang, C. Tao, C. Wang, B. Li, Z. Ni and S. Zhuang, *Opt. Lett.*, 2011, **36**, 4698–4700.
4 G. Zhang, C. Wang, B. Cao, Z. Huang, J. Wang, B. Zhang and K. Xu, *Opt. Express*, 2010, **18**, 7019–7030.
5 Y. T. Yoon, C. H. Park and S. S. Lee, *Appl. Phys. Express*, 2012, **5**, 022501.
6 Y. T. Yoon and S. S. Lee, *Opt. Express*, 2010, **18**, 534–549.
7 C. H. Park, Y. T. Yoon and S. S. Lee, *Opt. Express*, 2012, **20**, 23769–23777.
8 G. Gao, W. Gao, E. Cannuccia, J. Taha-Tijerina, L. Balicas, A. Mathkar, T. N. Narayanan, Z. Liu, B. K. Gupta, J. Peng, Y. Yin, A. Rubio and P. M. Ajayan, *Nano Lett.*, 2012, **12**, 3518–3525.
9 M. Bloemer and M. Scalora, *Appl. Phys. Lett.*, 1998, **72**, 1676–1678.
10 M. Scalora, M. J. Bloemer, A. C. Pethel, J. P. Dowling, C. M. Bowden and A. S. Manka, *J. Appl. Phys.*, 1998, **83**, 2377–2383.
11 Y. C. Lin, Z. J. Gao, Z. A. Chen, W. T. Yen and J. P. Huang, *Nanosci. Nanotechnol. Lett.*, 2009, **1**, 1–3.
12 J. Wu, W. Shen, H. Li, X. Liu and P. Gu, *Chin. Opt. Lett.*, 2010, **8**, 32–34.
13 H. Cho, C. Yun, J. W. Park and S. Yoo, *Org. Electron.*, 2009, **10**, 1163–1169.
14 M. C. Larciprete, C. Sibilia, S. Paoloni, M. Bertolotti and F. Sarto, *J. Appl. Phys.*, 2003, **93**, 5013–5017.
15 M. C. Zhang, T. W. Allen, B. Drobot, S. McFarlane, A. Meldrum and R. G. DeCorby, *Appl. Opt.*, 2013, **52**, 7479–7485.
16 T. Xu, Y. K. Wu, X. Luo and L. J. Guo, *Nat. Commun.*, 2010, **1**, 59.
17 B. Zeng, X. Yang, C. Wang and X. Luo, *Opt. Express*, 2009, **17**, 16783–16791.
18 T. Xu, L. Fang, J. Ma, B. Zeng, Y. Liu, J. Cui, C. Wang, Q. Feng and X. Luo, *Appl. Phys. B: Lasers Opt.*, 2009, **97**, 175–179.
19 J. A. Dionne, L. A. Sweatlock and H. A. Atwater, *Phys. Rev. B: Condens. Matter Mater. Phys.*, 2006, **73**, 035407.
20 K. T. Lee, S. Seo, J. Y. Lee and L. J. Guo, *Adv. Mater.*, 2014, **26**, 6324–6328.
21 H. A. Macleod, *Thin Film Optical Filters*, Optics and Optoelectronics Series, Institute of Physics Publishing, Bristol, England, 2003.
22 J. Cheng, D. B. Fan, H. Wang, B. W. Liu, Y. C. Zhang and H. Yan, *Semicond. Sci. Technol.*, 2003, **18**, 676–679.
23 E. D. Palik, *Handbook of Optical Constants of Solids*, Academic Press, San Diego, CA, 1998.
24 G. Leftheriotis, S. Papaefthimiou and P. Yianoulis, *Solid State Ionics*, 2000, **655**, 136–137.
25 M. Kawamura, Y. Abe and K. Sasaki, *Thin Solid Films*, 2006, **515**, 540–542.
26 M. K. Sinha, S. K. Mukherjee, B. Pathak, R. K. Paul and P. K. Barhai, *Thin Solid Films*, 2006, **515**, 1753–1757.
27 H. Pang, Y. Yuan, Y. Zhou, J. Lian, L. Cao, J. Zhang and X. Zhou, *J. Lumin.*, 2007, **122**, 587–589.
28 X. Liu, X. Cai, J. Qiao, J. Mao and N. Jiang, *Thin Solid Films*, 2003, **441**, 200–206.
29 X. Liu, X. Cai, J. Mao and C. Jin, *Appl. Surf. Sci.*, 2001, **183**, 103–110.
30 G. Kedawat, B. K. Gupta, P. Kumar, J. Dwivedi, A. Kumar, N. K. Agrawal, S. S. Kumar and Y. K. Vijay, *ACS Appl. Mater. Interfaces*, 2014, **6**, 8407–8414.
31 R. Vasireddy, R. Paul and A. K. Mitra, *Nanomater. Nanotechnol.*, 2012, **2**, 1–6.
32 M. W. Knight, L. Liu, Y. Wang, L. Brown, S. Mukherjee, N. S. King, H. O. Everitt, P. Nordlander and N. J. Halas, *Nano Lett.*, 2012, **12**, 6000–6004.
33 A. Paul, Y. Zhen, Y. Wang, W. Chang, Y. Xia, P. Nordlander and S. Link, *Nano Lett.*, 2014, **14**, 3628–3633.
34 W. L. Barnes, A. Dereux and T. W. Ebbesen, *Nature*, 2003, **424**, 824–830.

35 S. Yokogawa, S. P. Burgos and H. A. Atwater, *Nano Lett.*, 2012, **12**, 4349–4354.
36 B. Zeng, Y. Gao and F. J. Bartoli, *Sci. Rep.*, 2013, **3**, 2840.
37 X. L. Hu, L. B. Sun, B. Shi, M. Ye, Y. Xu, L. S. Wang, J. Zhao, X. L. Li, Y. Q. Wu, S. M. Yang, R. Z. Tai, H. J. Fecht, J. Z. Jiang and D. X. Zhang, *J. Appl. Phys.*, 2014, **115**, 113104.
38 G. Kedawat, S. Srivastava, V. K. Jain, P. Kumar, V. Kataria, Y. Agrawal, B. K. Gupta and Y. K. Vijay, *ACS Appl. Mater. Interfaces*, 2013, **5**, 4872–4877.
39 M. Lin, T. Sudhiranjan, C. Boothroyd and K. P. Loh, *Chem. Phys. Lett.*, 2004, **400**, 175–178.
40 H. V. Chung, P. T. Huy, T. T. An, N. T. M. Thuy and N. D. Chien, *J. Korean Phys. Soc.*, 2008, **52**, 1562–1565.